

Rapid and brief communication

## Multisets mixture learning-based ellipse detection

Zhi-Yong Liu<sup>a,b</sup>, Hong Qiao<sup>a</sup>, Lei Xu<sup>b,\*</sup>

<sup>a</sup>Key Lab of Complex Systems and Intelligence Science, Institute of Automation, Chinese Academy of Sciences, Beijing, China

<sup>b</sup>Department of Computer Science and Engineering, The Chinese University of Hong Kong, Shatin, N.T., Hong Kong, China

Received 9 June 2005; received in revised form 25 November 2005; accepted 29 November 2005

### Abstract

We develop an ellipse detection algorithm based on the multisets mixture learning (MML) that differs from the conventional Hough transform perspective. The algorithm developed has potential advantages in terms of noise resistance, incomplete ellipse detection, and detecting a multitude of ellipses.

© 2005 Pattern Recognition Society. Published by Elsevier Ltd. All rights reserved.

*Keywords:* Ellipse detection; Multisets mixture learning; Hough transform

### 1. Introduction

Ellipse detection in image is a basic task in pattern recognition and computer vision. It is usually accomplished by the Hough transform (HT) that involves a heavy computational load and a large storage requirement since it needs a five-dimensional parameter space. By adopting the randomized Hough transform (RHT) [1,2] and taking advantage of the symmetry or other particular properties of the ellipse, the time and space complexities can be considerably reduced. However, how to correctly detect the true peaks in the parameter space remains a tough task for the HT and its variants due to the uncertainties in image. Moreover, since for one curve concerned, the pixels of the remaining curves act just as *noises*, the HT-based methods suffer from a poor scalability of detecting a multitude of curves.

This paper solves the ellipse detection via the multisets mixture learning (MML) [3], which is a totally different perspective from the HT. The MML, proposed as a unified learning framework for supervised and unsupervised learning, provides a new viewpoint for object detection by minimizing the sample reconstruction error upon each object. When used for curve detection and in comparison with the HT-based approaches, it has advantages in terms of noise

resistance and scalability of detecting a multitude of curves. In Section 2 we review the MML-based curve detection method and develop an ellipse detection algorithm. In Section 3 we experimentally demonstrate the algorithm and finally we conclude in Section 4.

### 2. Multisets mixture learning for ellipse detection

Given a data sample set  $U = \{\mathbf{u}_t\}_{t=1}^N$  that comes from  $k$  curves, denoted by  $S_i(\theta_i)$  ( $i = 1, \dots, k$ ), plus random noises, as illustrated by Fig. 1, the MML estimates the parameters  $\Theta = \{\theta_i\}_{i=1}^k$  via minimizing the square reconstruction error  $E$  of the samples as follows [3]:

$$\Theta = \arg \min_{\Theta} E, \quad E = \sum_{i=1}^k E_i, \quad E_i = \sum_{\mathbf{u}_t \in U_i} e_i(\mathbf{u}_t),$$

$$e_i(\mathbf{u}_t) = \|\mathbf{u}_t - \hat{\mathbf{u}}_{i,t}\|^2, \quad (1)$$

where  $e_i(\mathbf{u}_t)$  and  $\hat{\mathbf{u}}_{i,t}$ , respectively, denote the reconstruction error and the best reconstruction of the sample  $\mathbf{u}_t$  upon curve  $i$ ,  $U_i$  denotes the set that consists of all the samples belonging to object  $i$ . Such estimated curves capture the main axis of the data samples, and it actually degenerates to detect the first principal component of the samples when the curve is constrained as a line.

To detect the ellipse under the framework of MML, we need first to find the sample reconstruction error upon an

\* Corresponding author. Tel.: 852 26098423.

E-mail address: [lxu@cse.cuhk.edu.hk](mailto:lxu@cse.cuhk.edu.hk) (L. Xu).

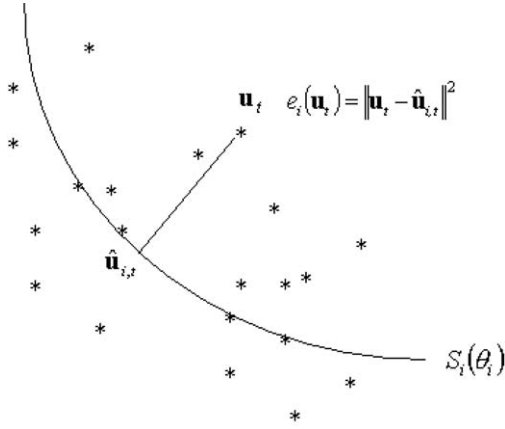
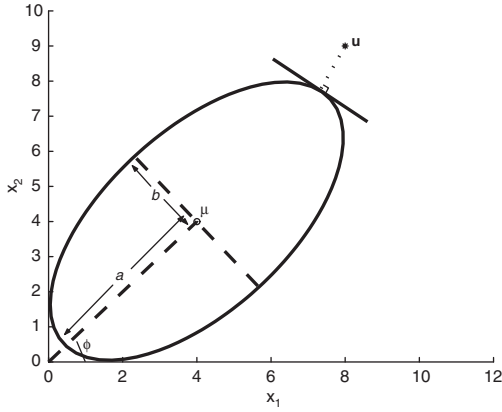


Fig. 1. Error between sample and curve.

Fig. 2. Distance between sample  $\mathbf{u}$  and ellipse.

ellipse. In general, an ellipse takes the following equation:

$$(\mathbf{x} - \boldsymbol{\mu})^T \boldsymbol{\Sigma} (\mathbf{x} - \boldsymbol{\mu}) = 1, \quad \boldsymbol{\Sigma} = \boldsymbol{\Phi}^T \mathbf{D} \boldsymbol{\Phi}, \quad (2)$$

where  $\boldsymbol{\mu} \in \mathbf{R}^2$  denotes the ellipse center,  $\boldsymbol{\Phi} \in \mathbf{R}^{2 \times 2}$  denotes a rotation matrix, and the positive-definite diagonal matrix  $\mathbf{D} \in \mathbf{R}^{2 \times 2}$  indicates the length of its two axes. For instance, the ellipse shown in Fig. 2 can be represented by Eq. (2) by setting  $\boldsymbol{\Phi} = [\cos \phi, \sin \phi; -\sin \phi, \cos \phi]^T$  and  $\mathbf{D} = [1/a^2, 0; 0, 1/b^2]$ . The reconstruction error  $e(\mathbf{u})$  of the sample  $\mathbf{u}$ , or equivalently the shortest distance between  $\mathbf{u}$  and the ellipse can be then found by solving the following constraint optimization problem:

$$\min_{\hat{\mathbf{u}}} e(\mathbf{u}) = \|\hat{\mathbf{u}} - \mathbf{u}\|^2 \quad \text{subject to} \quad (\hat{\mathbf{u}} - \boldsymbol{\mu})^T \boldsymbol{\Sigma} (\hat{\mathbf{u}} - \boldsymbol{\mu}) = 1 \quad (3)$$

whose Lagrangian function is obtained as follows:

$$L(\hat{\mathbf{u}}, \lambda) = \|\hat{\mathbf{u}} - \mathbf{u}\|^2 - \lambda [(\hat{\mathbf{u}} - \boldsymbol{\mu})^T \boldsymbol{\Sigma} (\hat{\mathbf{u}} - \boldsymbol{\mu}) - 1]. \quad (4)$$

The  $\hat{\mathbf{u}}$  that minimizes Eq. (3) should satisfy two points. First, it is a stationary point of Eq. (4), and second, it leads to the Hessian matrix of Eq. (4), positive definite. The stationary

point can be obtained by making the derivative of  $L(\hat{\mathbf{u}}, \lambda)$  with respect to  $\hat{\mathbf{u}}$  to be zero, i.e.

$$\frac{\partial L(\hat{\mathbf{u}}, \lambda)}{\partial \hat{\mathbf{u}}} = 2(\hat{\mathbf{u}} - \mathbf{u}) - 2\lambda \boldsymbol{\Phi}^T \mathbf{D} \boldsymbol{\Phi} (\hat{\mathbf{u}} - \boldsymbol{\mu}) = 0$$

$$\Rightarrow \hat{\mathbf{u}} = (\lambda \boldsymbol{\Sigma} - I)^{-1} (\lambda \boldsymbol{\Sigma} \boldsymbol{\mu} - \mathbf{u}), \quad (5)$$

$$\Rightarrow e(\mathbf{u}) = \|(\lambda \boldsymbol{\Sigma} - I)^{-1} (\lambda \boldsymbol{\Sigma} \boldsymbol{\mu} - \mathbf{u}) - \mathbf{u}\|^2, \quad (6)$$

where the  $\lambda$  can be found via replacing the  $\mathbf{x}$  in Eq. (2) by  $\hat{\mathbf{u}}$  as follows:

$$f(\lambda) = 1 - (\hat{\mathbf{u}} - \boldsymbol{\mu})^T \boldsymbol{\Sigma} (\hat{\mathbf{u}} - \boldsymbol{\mu}) = 0 \quad (7)$$

with  $\hat{\mathbf{u}}$  given by Eq. (5). The solution of Eq. (7) should resort to numerical techniques due to its analytical intractability. Here we adopt the Newton's iteration scheme by finding

$$f'(\lambda) = 2((\lambda \boldsymbol{\Sigma} - I)^{-1} (\lambda \boldsymbol{\Sigma} \boldsymbol{\mu} - \mathbf{u}) - \boldsymbol{\mu})^T \boldsymbol{\Sigma} (\lambda \boldsymbol{\Sigma} - I)^{-1} \times \boldsymbol{\Sigma} ((\lambda \boldsymbol{\Sigma} - I)^{-1} (\lambda \boldsymbol{\Sigma} \boldsymbol{\mu} - \mathbf{u}) - \boldsymbol{\mu}).$$

The Hessian matrix of Eq. (4) is

$$\nabla_{\hat{\mathbf{u}}}^2 L(\hat{\mathbf{u}}, \lambda) = 2\boldsymbol{\Phi}^T (I - \lambda \mathbf{D}) \boldsymbol{\Phi}.$$

To make it positive definite, the  $\lambda$  must satisfy

$$\lambda < \frac{1}{D_{big}}, \quad D_{big} = \max\{D_{11}, D_{22}\},$$

since  $\mathbf{D}$  is a positive-definite diagonal matrix. It can be guaranteed by introducing the line search procedure, e.g., the cubic polynomial method, or simply the form  $\lambda = 1/D_{big} - e^\zeta$  with another variable  $\zeta$ .

As the sample reconstruction error has been obtained, Eq. (1) can be performed to detect ellipse. We choose the rival penalized competitive learning (RPCL) for Eq. (1), which mathematically consists of the following two steps [4,3]:

**Step 1:** For the sample  $\mathbf{u}_t$ , find the winner cluster  $i_c$  and the rival one  $i_r$  as follows:

$$i_c = \arg \min_i \gamma_i e_i(\mathbf{u}_t), \quad i_r = \arg \min_{i \neq i_c} \gamma_i e_i(\mathbf{u}_t),$$

$$\gamma_i = \frac{n_i}{\sum_{j=1}^k n_j}, \quad (8)$$

where  $n_j$  denotes the cumulative times of the cluster  $j$  being winner.

**Step 2:** Update the parameters as follows:

$$\theta_{i_c}^{new} = \theta_{i_c}^{old} - \eta_c \nabla_{\theta_{i_c}} e_{i_c}(\mathbf{u}_t), \quad \theta_{i_r}^{new} = \theta_{i_r}^{old} + \eta_r \nabla_{\theta_{i_r}} e_{i_r}(\mathbf{u}_t),$$

$$\theta_i = \{\mu_i, \boldsymbol{\Phi}_i, \mathbf{D}_i\}, \quad (9)$$

where  $\nabla_{\theta_i} e_i(\mathbf{u})$  denotes the derivative of  $e_i(\mathbf{u})$  with respect to  $\theta_i$ , and the learning rate  $\eta_c$  is much larger than the de-learning rate  $\eta_r$ .

Learning via RPCL will not only possess model selection ability by pushing the redundant cluster centers far away from the data, but also avoid the dead unit trouble for clustering due to the introduced conscience and de-learning mechanisms [4].

Based on the reconstruction error  $e(\mathbf{u})$  of sample  $\mathbf{u}$  given by Eq. (6), the specific updating forms for  $\{\mu, \mathbf{D}, \Phi_i\}$  in step 2 are obtained as follows:

$$\nabla_{\mu_i} e_i(\mathbf{u}) = 2\lambda_i \Sigma_i \Gamma_i \mathbf{g}_i, \tag{10}$$

$$\nabla_{\mathbf{D}_i} e_i(\mathbf{u}) = 2\lambda_i \text{diag}[\Phi_i \Gamma_i \mathbf{g}_i (\mu_i - \mathbf{g}_i - \mathbf{u})^T \Phi_i^T], \tag{11}$$

$$\begin{aligned} \nabla_{\Phi_i} e_i(\mathbf{u}) = & 2\lambda_i \mathbf{D}_i \Phi_i [(\mu_i - \mathbf{g}_i - \mathbf{u}) \mathbf{g}_i^T \Gamma_i \\ & + \Gamma_i \mathbf{g}_i (\mu_i - \mathbf{g}_i - \mathbf{u})^T], \end{aligned} \tag{12}$$

where  $\mathbf{g}_i = \Gamma_i (\lambda_i \Sigma_i \mu_i - \mathbf{u}_i) - \mathbf{u}_i$ ,  $\Gamma_i = (\lambda_i \Sigma_i - I)^{-1}$ . In practice we can introduce  $\mathbf{D}_i = e^{\Omega_i}$  to guarantee the diagonal matrix  $\mathbf{D}_i$  is positive definite, where  $\Omega_i$  is a diagonal matrix. For the  $\Phi$  which is under the orthonormality constraint, its updating along the geodesic on the Stiefel manifold is as follows [5]:

$$\begin{aligned} \Phi_i(\tau) &= \Phi_i \mathbf{M}(\tau) + \mathbf{Q}\mathbf{N}(\tau), \\ \begin{pmatrix} \mathbf{M}(\tau) \\ \mathbf{N}(\tau) \end{pmatrix} &= \exp \left\{ \tau \begin{pmatrix} \mathbf{A} & -\mathbf{R}^T \\ \mathbf{R} & \mathbf{0} \end{pmatrix} \right\} \begin{pmatrix} \mathbf{I}_p \\ \mathbf{0} \end{pmatrix}, \\ \mathbf{A} &= \Phi_i^T \mathbf{H}, \quad \mathbf{H} = \Phi_i (\nabla_{\Phi_i} e_i(\mathbf{u}))^T \Phi_i - \nabla_{\Phi_i} e_i(\mathbf{u}), \\ \mathbf{Q}\mathbf{R} &= (\mathbf{I} - \Phi_i \Phi_i^T) \mathbf{H} (\Phi_i)^T \text{ is the compact QR decomposition,} \end{aligned} \tag{13}$$

where  $\tau$  takes the same role as the learning rate  $\eta$  in Eq. (9).

Finally, we summarize the three steps for the ellipse detection as follows:

*Step 1:* for sample  $\mathbf{u}_t$ , find  $\{\lambda_i\}_{i=1}^k$  by the Newton's iteration scheme,

*Step 2:* perform the first step of RPCL shown in Eq. (8),

*Step 3:* perform the second step of RPCL shown in Eq. (9). If converged, stop; otherwise, go to step 1.

### 3. Preliminary experiments and discussions

We now demonstrate the ability of the algorithm developed on (1) noise resistance ability, (2) ability of detecting incomplete ellipses, and (3) scalability in terms of detecting a multitude of ellipses. Meantime, we choose the standard HT-based algorithm and RHT-based algorithm [2] for comparison, and both MML and RHT-based algorithms are randomly repeated 20 times.

The three synthetic images adopted for demonstrating the noise resistance are characterized, noise-free, moderate noise and heavy noise shown in Fig. 3. The results obtained are listed in Table 1, where we present the maximum, minimum and average number of ellipses detected in the 20 runs of the MML and RHT-based algorithms. For saving the space, the visual experiment results are not shown here. As shown by the results, the performance of the MML-based algorithm is quite insensitive to noise. The results could be contrasted with HT and RHT-based algorithms whose performance deteriorates as noise level increases. A possible explanation for such differences may be as follows. For ellipse detection, the MML-based algorithm captures the main axis

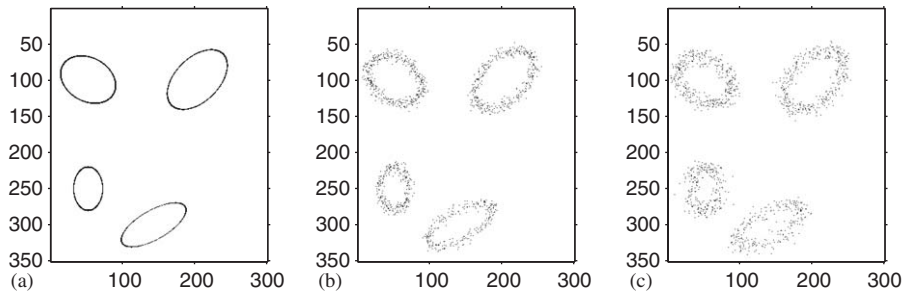


Fig. 3. Synthetic images containing different noise levels used in the experiment: (a) noise free, (b) moderate noise, and (c) heavy noise.

Table 1  
Comparisons on performance by different algorithms

	MML (20 runs)			HT	RHT (20 runs)		
	Min	Max	Mean		Min	Max	Mean
Fig. 3							
(a) Noise free	3	4	3.8	4	3	4	3.9
(b) Moderate noise	2	4	3.7	2	1	4	2.7
(c) Heavy noise	3	4	3.8	0	0	2	0.9
Fig. 4 (5 ellipses)	2	5	4.3	1	0	2	1.5
Fig. 6 (11 ellipses)	4	11	8.6	2	1	10	6.5

Min, max and mean denote the minimum, maximum and average number of ellipses detected, respectively.

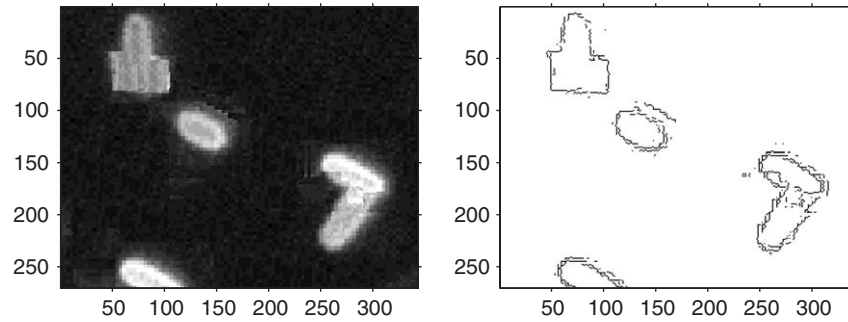


Fig. 4. Five incomplete elliptic bacteria before and after edge detection.

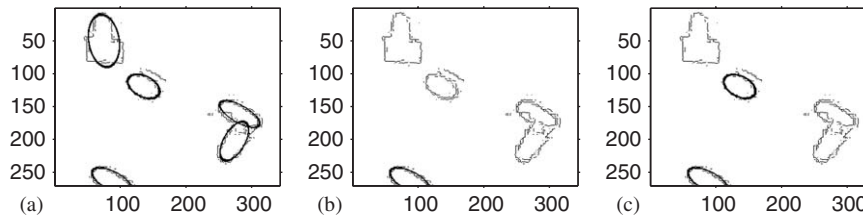


Fig. 5. Typical results by different algorithm on incomplete ellipse detection: (a) 5 ellipses detected by MML, (b) 1 ellipse detected by HT, and (c) 2 ellipses detected by RHT.

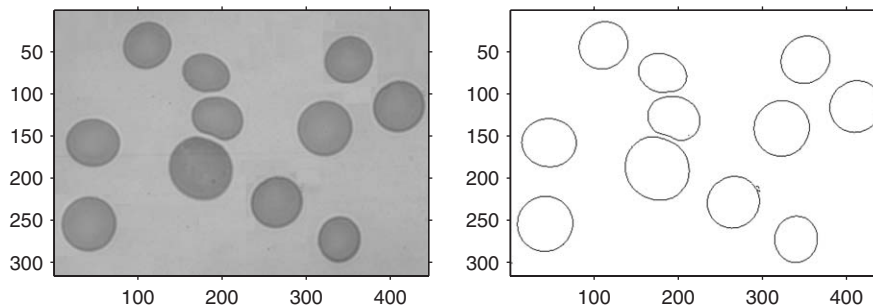


Fig. 6. Eleven elliptic blood cells before and after edge detection.

of the ellipses by minimizing the total reconstruction error. Thus, its performance is insensitive to the noise as long as the main axis of the data samples can be traced. However, for the HT and RHT-based algorithms, the patterns transformed by the noise would submerge the true peaks in the parameter space as the noise level increases. The RHT has a better noise resistance ability than the HT because the RHT can increase the resolution of parameterization and the robustness to outliers [1].

The image used for the incomplete ellipse detection is a real biological image that contains five elliptic bacteria, of which four are incomplete, as shown in Fig. 4. Among the four incomplete bacteria, the top one is almost half curtailed by the rectangle-shape noise, the bottom one only leaves half due to the improper image cut, and the other two are interlaced together. Experimental results are tabulated in Table 1 and illustrated in Fig. 5. While the MML-based algorithm is capable of detecting 4.3 ellipses on average, the HT and

RHT can only detect 1 and 1.5 ellipses, respectively. The fact that the MML-based algorithm outperforms its counterparts could also be explained by the strategy of capturing the main axis of samples. For example, although the top incomplete ellipse is contaminated by the rectangle-shape noise, the axis of the samples detected by the MML-based algorithm would still roughly represent the original ellipse. On the other hand, such a contaminated ellipse can hardly create an effective peak in the parameter space for the HT or RHT-based algorithms.

The image shown in Fig. 6 is adopted to demonstrate the scalability of the algorithms, which is a real world image containing 11 elliptic blood cells pre-processed by edge detection. Results are provided in Table 1. As shown in Table 1, the MML-based algorithm outperforms its counterparts by detecting 8.6 ellipses on average while the RHT and HT detect only 6.5 and 2 ellipses, respectively. Actually, the difficulties facing different algorithms on detecting

a multitude of ellipses are not the same. The major difficulty underlying the MML-based algorithm originates from the so-called “dead unit” problem, due to the existence of some *empty* cluster centers that cannot occupy any samples. However, the MML-based algorithm overcomes this problem by introducing the conscience and de-learning mechanisms with the help of the RPCL. On the other hand, as the HT and RHT-based algorithms are employed to detect a particular ellipse in the presence of many other ellipses, pixels of other ellipses would unavoidably pose as *noises* to worsen their performance.

#### 4. Conclusion

An ellipse detection algorithm is developed based on the multisets mixture learning and it differs from the viewpoint of HT family. The algorithm is shown experimentally and analytically to have certain advantages over the conventional approaches.

#### Acknowledgements

The work described in this paper was fully supported by a grant from the Research Grant Council of the Hong Kong SAR (Project no: CUHK4225/04E).

#### References

- [1] L. Xu, E. Oja, Randomized hough transform (RHT): basic mechanisms, algorithms and complexities, *Comput. Vision, Graphics, Image Process.: Image Understanding* 57 (2) (1993) 131–154.
- [2] R.A. McLaughlin, Randomized Hough transform: improved ellipse detection with comparison, *Pattern Recogn. Lett.* 19 (1998) 299–305.
- [3] L. Xu, Data smoothing regularization, multi-sets-learning, and problem solving strategies, *Neural Networks* 16 (5–6) (2003) 817–825.
- [4] L. Xu, A. Krzyzak, E. Oja, Rival penalized competitive learning for clustering analysis, RBF net, and curve detection, *IEEE Trans. Neural Networks* 4 (1993) 636–649.
- [5] A. Edelman, T.A. Arias, S.T. Smith, The geometry of algorithms with orthogonality constraints, *SIAM J. Matrix Anal. Appl.* 20 (2) (1998) 303–353.